Assessing the Stability of Alzheimer's Amyloid Protofibrils Using Molecular Dynamics

Justin A. Lemkul and David R. Bevan*

Department of Biochemistry, 111 Engel Hall, Virginia Polytechnic Institute and State University, Blacksburg, Virginia 24061-0308

Received: November 21, 2009; Revised Manuscript Received: December 21, 2009

Amyloid fibrils represent a stable form of many misfolded proteins associated with numerous diseases. Among these are Parkinson's disease (α-synuclein), Type II diabetes (islet amyloid polypeptide), and Alzheimer's disease (amyloid β-peptide, Aβ). The appearance of Aβ fibrils in neural tissue is a hallmark of Alzheimer's disease, and many studies have been conducted to determine and analyze the structure of these protein aggregates. The principal toxic species in Alzheimer's disease are believed to be soluble, oligomeric aggregates of Aβ, but numerous studies have found that the insoluble fibrillated form of the peptide also contributes to neurotoxicity. Thus, to design therapeutic agents to combat the progression of Alzheimer's disease, it is worthwhile to understand the thermodynamics of destabilizing these aggregates and the features that contribute to their stability. In this work, we present a systematic study of several factors that influence the stability of $A\beta_{42}$ fibrils following in silico mutation. We have employed standard molecular dynamics, as well as center-of-mass pulling and umbrella sampling, to study the thermodynamics of peptide dissociation from the core of a model protofibril at physiological temperature. Results indicate that a finite level of hydration around the Asp23−Lys28 salt bridge is crucial to protofibril stability, while mutation of Phe19 to glycine has no effect on the binding free energy of the terminal peptide. Packing between Ile32 and the aliphatic portion of the Lys28 side chain serves to regulate the level of hydration in the core of the protofibril and thus rigidify the Asp23−Lys28 salt bridge. These observations are important for designing compounds that target Aβ aggregates; interrupting these native interactions may destabilize these assemblies and ameliorate their toxicity.

Introduction

Alzheimer's disease is the leading cause of senile dementia, afflicting upward of 5 million Americans and 25 million individuals worldwide.[1] In the absence of effective therapeutics, these numbers are likely to increase rapidly as the population ages. Hallmark symptoms of Alzheimer's disease include memory loss, impaired learning and general cognition, and dementia. Although the underlying cause of Alzheimer's disease is not completely clear, it is apparent that the symptoms of this disease are manifested as a result of the aggregation and deposition of amyloid β-peptide (Aβ) in neural tissue. The connection between Aβ and Alzheimer's disease has become known as the "amyloid hypothesis."[2]

The Aβ peptide is derived from the amyloid precursor protein (APP) by sequential cleavage of β- and γ-secretases to give a membrane-bound peptide.[3] The length of the peptide is variable, from 39 to 43 amino acids, with the most prominent forms of the peptide being 40 and 42 residues in length. In healthy individuals, $A\beta_{40}$ comprises approximately 90% of the total Aβ.[4] In the disease state, the ratio of $A\beta_{42}$:$A\beta_{40}$ is elevated, leading to increased amyloid deposition over time, since the $A\beta_{42}$ variant more readily forms aggregates in solution.[3] A number of Aβ assemblies have been identified, from small dimeric and trimeric species to soluble oligomers, annular assemblies, protofilaments, and insoluble plaques composed of the mature fibril.[3] $A\beta_{42}$ comprises the major form of Aβ found in plaques.[4]

Numerous studies have been conducted to investigate the mechanism of Aβ toxicity. It has become clear that soluble oligomers, amorphous in shape and lacking well-defined secondary structure, are the most cytotoxic forms of Aβ.[5−8] However, it is important to note that exposure of cultured neurons to preformed Aβ fibrils results in cell death,[9−12] and pro-oxidant metals are found in high quantities in amyloid plaques, suggesting that plaque formation may contribute to the oxidative stress present in the Alzheimer's brain.[13] Moreover, histological investigations have found that Aβ plaques are surrounded by dystrophic neurites,[4] indicating that Aβ fibrils are also neurotoxic and not simply an inert byproduct of Aβ accumulation. The fact that Aβ fibrils may contribute in some way to the neurotoxicity in Alzheimer's disease makes these proteinaceous aggregates an attractive target for therapeutics.

Whereas the structure of oligomeric Aβ is not rigorously defined, the structure of the Aβ fibril has been studied extensively, primarily by nuclear magnetic resonance (NMR) spectroscopy.[9,14−16] Different structural models have been proposed from these data, based on the principal form of Aβ in the fibril, either $A\beta_{42}$ or $A\beta_{40}$. The resulting models provide important details necessary for studying the mechanism by which these species may be destabilized in an effort to dissolve the fibrils.

Molecular dynamics (MD) simulations have been successfully used to study interactions among proteins, lipids, and small molecules and provide atomic-level detail of many phenomena. Due to the inherent difficulty of obtaining high-resolution structural data of Aβ aggregates and their assembly or disassembly, MD simulations are an ideal tool for studying these systems. An especially useful technique in analyzing macromolecular interactions is umbrella sampling.[17−19] In this method, a series of configurations is generated along a reaction coordinate, ξ, between two interacting species. One of these species serves as a reference, while the other group is placed at

* Corresponding author. E-mail: drbevan@vt.edu. Phone: (540) 231-5040. Fax: (540) 231-9070.

10.1021/jp9110794
Published on Web 01/07/2010

increasing center-of-mass (COM) distance from the reference with its position maintained by a biasing potential. These COM distances represent so-called "sampling windows," wherein independent simulations are conducted to generate an ensemble of structures along the reaction coordinate. Within each of these windows, values of the potential of mean force (PMF) can be calculated. To assemble a PMF curve as a function of the entire reaction coordinate (ξ), energy values in adjacent windows are reassembled such that they produce a continuous function.

Although numerous MD studies have examined the basis for the stability of Aβ_{40} fibril,[20−23] the principal form of Aβ in the disease state is Aβ_{42}.[4] Thus, it is critical to understand the structural basis for the stability of Aβ_{42} fibrils, as well. Here, we present the results of COM pulling and umbrella sampling simulations using an atomistic model of a pentameric Aβ protofibril in explicit solvent at physiological temperature. The details described herein can be used for targeted drug design of compounds that are able to interrupt the most essential interactions within the Aβ fibril.

Methods

The model for the Aβ fibril chosen for this work was the core of the Aβ_{42} fibril, a protofilament structure determined using solid-state NMR.[9] In this model (PDB code 2BEG), the N-terminal 16 amino acids are missing. Masman et al. recently proposed that this core region of the fibril, comprising residues 17−42, is principally responsible for its stability.[24] As such, although only a portion of the Aβ protofilament, and thus the larger fibril as a whole, was modeled here, the observations made and conclusions reached likely extend to the mature, full-length Aβ fibril. Due to the small size of the assembly considered here (five peptides), the structure will be referred to as a "protofibril," as it is the structure that comprises the repeat unit of a protofilament, and ultimately the mature fibril. A representative structure, containing intact salt bridges, was chosen from the ensemble of structures in the PDB file as the starting structure for the simulations in this work. The mutants considered in this work are denoted F19G, D23A, K28A, and the double mutant I32G/L34G. These in silico mutations were made by simply deleting appropriate side-chain atoms, leaving only the β-carbon in the case of alanine mutants, and no side-chain atoms in the case of glycine mutants. The mutation of Phe19 to glycine was motivated by the structural studies of Lührs et al., who found that, despite the mutation, the Aβ F19G mutant formed fibrils, albeit of distinct morphology from the wild type.[9] The mutations of Asp23 and Lys28 to alanine were an attempt to assess the contribution of the interpeptide salt bridges present in the hydrophobic core to the stability of the fibril by removing this favorable electrostatic interaction. Several studies have suggested the formation of this salt bridge contributes strongly to the stability of amyloid aggregates as higher-order structures develop.[25−27] The choice of mutating these residues to alanine was motivated by standard biochemical techniques (such as alanine scanning mutagenesis) for assessing side-chain function. By mutating Ile32 and Leu34 to glycine, we sought to probe hydrophobic packing interactions that may contribute to stabilizing the salt bridge and the hydrophobic interior of the fibril. Glycine was chosen for these mutations instead of alanine to eliminate potential hydrophobic contacts involving the β-carbon of alanine. It is not implied that any of these mutants should necessarily form fibrils, but these mutations are relevant here in the assessment of side-chain contributions to stability.

The N-terminus of each peptide was capped with an acetyl group to give an uncharged terminus to mimic the full-length peptide, wherein additional amino acids would be present. The C-terminus of each peptide was deprotonated (−1 charge). All other titratable amino acids were assigned their canonical state at physiological pH. Parameters from the GROMOS96 53A6 parameter set[28] were applied to all species in the simulated system. Short-range nonbonded interactions were cut off at 1.4 nm, with long-range electrostatics calculated using the particle mesh Ewald (PME) algorithm.[29,30] Dispersion correction was applied to energy and pressure terms to account for truncation of van der Waals terms. Periodic boundary conditions were applied in all directions.

In order to generate equilibrated starting structures for the pulling simulations, each protofibril (wild type and mutants) was placed in a cubic box of simple point charge (SPC) water,[31] to which 100 mM NaCl was added, including neutralizing counterions. Following steepest descents minimization, each of the protofibril systems was equilibrated in two steps, with position restraints applied to peptide heavy atoms throughout. The first phase involved simulating for 50 ps under a constant volume (NVT) ensemble. Protein and nonprotein atoms were coupled to separate temperature coupling baths, and temperature was maintained at 310 K using the Berendsen weak coupling method.[32] Following NVT equilibration, 50 ps of constant-pressure (NPT) equilibration were performed, also using weak coupling[32] to maintain pressure isotropically at 1.0 bar. Production MD simulations were conducted for 100 ns in the absence of any restraints. For this data collection period, the Nosé−Hoover thermostat[33,34] was used to maintain temperature, and the Parrinello−Rahman barostat[35,36] was used to isotropically regulate pressure. This combination of thermostat and barostat ensures that a true NPT ensemble is sampled.[33−36] Simulations were conducted using the GROMACS package, version 4.0.2.[37]

Structures from the end of each of these trajectories (WT, F19G, I32G/L34G, K28A, and D23A) were used as starting configurations for pulling simulations. The protofibril structures were placed in a rectangular box with dimensions sufficient to satisfy the minimum image convention and provide space for pulling simulations to take place along the z-axis. As before, SPC water was used to represent solvent, and 100 mM NaCl was present in the simulation cell. All pulling simulations were conducted with the GROMACS package, version 4.0.4, to take advantage of pull code improvements and new features implemented during the course of the project. Equilibration was performed for 100 ps under an NPT ensemble, using the same methodology described above.

Following equilibration, restraints were removed from all peptides except peptide B (Figure 1); it was used as an immobile reference for the pulling simulations. Position restraints have frequently been used in simulations of model Aβ fibrils to mimic the stability of a much larger structure.[20,21,38] For each of the protofibril structures, peptide A was pulled away from the core structure along the z-axis (Figure 1) over 500 ps, using a spring constant of 1000 kJ mol^{-1} nm^{-2} and a pull rate of 0.01 nm ps^{-1} (0.1 Å ps^{-1}). Application of slower pulling rates (0.005 and 0.001 nm ps^{-1}) resulted in the production of nearly identical trajectories and similar force vs time curves (see Figure S1, Supporting Information), and thus the faster pulling rate was applied to all systems here in order to expedite data collection while still preserving reliability of the results. A final center-of-mass (COM) distance between peptides A and B of approximately 5.5 nm was achieved. From these trajectories, snapshots were taken to generate the starting configurations for the umbrella sampling[17−19] windows. An asymmetric distribution of sampling windows was used, such that the window spacing

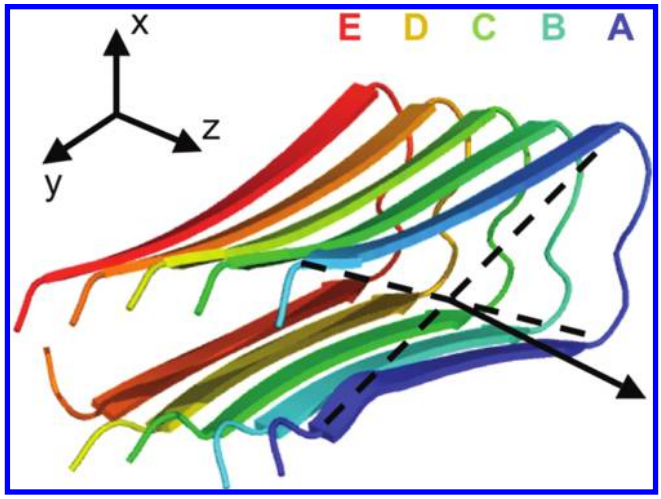

Figure 1. Aβ_{42} protofilament structure from NMR,[9] with each peptide colored and labeled according to the nomenclature used in this paper. Peptide A corresponds to the "growing end" proposed by Lührs et al. to explain the apparent unidirectional growth of amyloid fibrils. Axes are shown to indicate the pulling direction, coincident with the fibril axis. The image was rendered with PyMOL.[55]

was 0.1 nm up to 2 nm COM separation, and 0.2 nm beyond 2 nm of COM separation. Such spacing allowed for increasing detail at smaller COM distance, and resulted in 31 windows. In each window, 10 ns of MD was performed for a total simulation time of 310 ns utilized for umbrella sampling. Analysis of results was performed with the weighted histogram analysis method (WHAM).[39]

Results

Throughout this report, all amino acids will be referred to by their position in the full-length Aβ peptide, for ease of reference to previous experiments, even though the N-terminal 16 residues were missing in the structure modeled here. The β-strands in the protofibril are referred to as β1 (extending from residues 18−26) and β2 (residues 31−42), from the nomenclature devised by Lührs et al.[9] A bend region connects the two β-strands.

Structural Details of Protofibrils from MD Simulations. Mutations in the Aβ sequence led to noticeable distortions in the structure of the protofibril over the course of 100 ns MD trajectories, although none of the peptides spontaneously dissociated from the core of the structure. Shown in Figure 2 are images of the starting structures used in the pulling simulations; these structures are the result of 100 ns of unrestrained MD following the equilibration protocol described above. Backbone root-mean-square deviation (rmsd) values are shown in Table 1. These values represent the average calculated over the period of the simulation during which the rmsd was stable, generally the last 50 ns. Maintenance of the integrity of the hydrophobic core of the protofibril explains the observed structures. From Figure 2a and Table 1, it can be seen that the wild-type protofibril did not deviate substantially from the original NMR structure. Also in the wild-type structure, the Asp23−Lys28 salt bridges were maintained over time in six independent simulations (data not shown). Mutation of Phe19 to glycine resulted in a pinched structure, with strand β2 making contact with strand β1 where the side chain of Phe19 normally packs against Gly38 (Figure 2b). Mutating Asp23 to alanine prompted the Lys28 residues of each peptide to orient their side chains into the aqueous solvent, thus removing the positively charged residues from the hydrophobic core (Figure 2c). This behavior led to minimal deformation of the protofibril structure. The K28A mutation caused the greatest changes to the protofibril structure. Since aspartate lacks a long, flexible side chain like that of lysine, this charged residue is less able to move outward to the aqueous environment to solvate the negatively charged carboxylate (Figure 2d). As such, the K28A protofibril, while still maintaining the overall integrity of its hydrophobic core, deforms substantially to maximize the exposure of Asp23 to solvent, which protrudes through the bend region into the solvent. In the case of the I32G/L34G mutant, the most significant observation is the increased solvation of the Asp23−Lys28 salt bridge, which leads to destabilization of the bend region (Figure 2e). In the WT protofibril, an average of 6.8 water molecules was present in the solvent-accessible channel near the Asp23−Lys28 salt bridges (Figure 3a), with a maximum solvation at times reaching 15 water molecules. In the case of the I32G/L34G mutant, an average of 7.8 water molecules was present over time, peaking at a maximum of 30 water molecules. For the F19G protofibril, an average of 5.1 water molecules was present per time frame, with solvation peaking at 13 water molecules. In the case of D23A, this solvent-accessible channel was absent due to the hydrophobic packing that evolved over the course of the 100 ns simulation. In the K28A protofibril, no solvent-accessible channel can be rigorously defined based on the structural changes that took place.

Twisting of β-strands in Aβ fibrils relative to one another to increase side-chain contacts (particularly in the β2 region) has been proposed as a driving force for amyloid fibril stability and has been observed in previous MD simulations.[23,24,40] We find that in all cases, some twisting is apparent (Figure 2) and side-chain contacts quickly increase (within 10 ns of simulation) and remain largely stable over the remainder of each of the trajectories (Figure S2, Supporting Information). We note that a previous study by Masman et al.[24] observed a more pronounced twisting effect in the case of the WT protofibril than is observed here (Figure 2a), a difference that may be attributed to the presence of additional residues in the previous study (full-length peptides instead of the truncated form utilized here) and the choice of force field used (OPLS-AA[41] in the previous work, and GROMOS96 53A6[28] in this study). Contacts formed between side-chain atoms in the β2 region are comparable among the WT, F19G, D23A, and K28A protofibrils, with F19G forming somewhat more contacts than the WT due to the pinching at the C-terminus described above (Figure S2, Supporting Information). The β2 region of the I32G/L34G mutant forms substantially fewer total side-chain contacts due to the instability of peptide E over the course of 100 ns of MD simulation. The most dramatic difference in terms of contacts are seen when considering the core residues that pack around the Asp23−Lys28 salt bridges, specifically residues 21−34, packing interactions whose importance will be described in the subsequent sections. While the F19G protofibril forms more contacts than any other protofibril in this core region, the other mutated structures (D23A, I32G/L34G, and K28A) form substantially fewer contacts than either the WT or F19G protofibrils (Figure S2, Supporting Information), which likely contributes to the instability seen in these structures.

Center-of-Mass Pulling Simulations. COM pulling, or steered molecular dynamics (SMD), simulations can be used to bias the behavior of a system toward a particular phenomenon that might otherwise be inaccessible on the time scale of conventional MD. SMD simulations have been successfully applied to the study of many processes, including protein−ligand binding, protein−protein interactions, and extraction of lipids

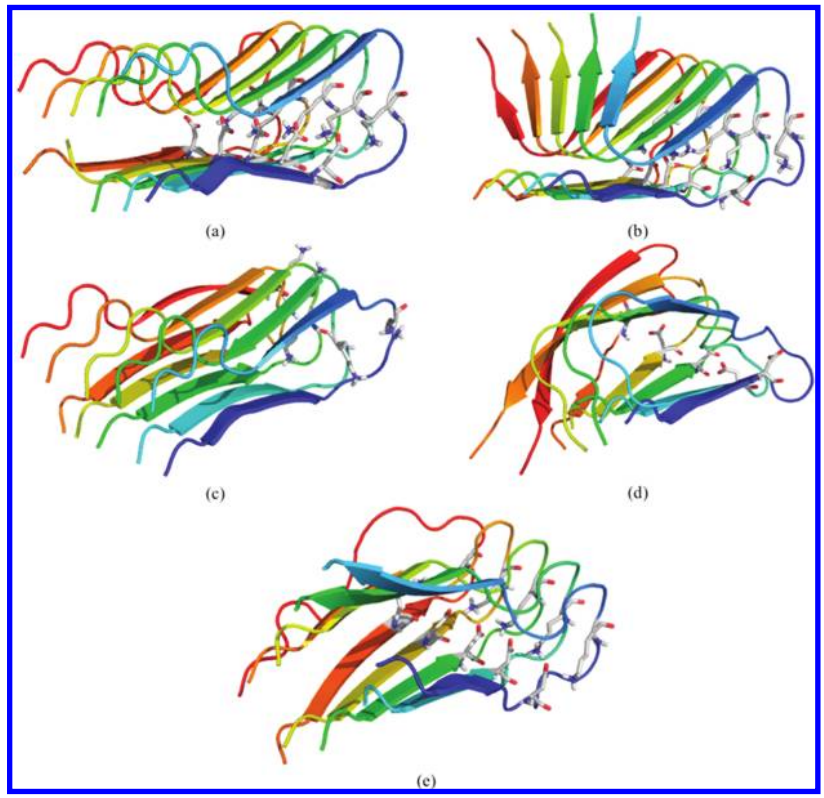

Figure 2. Protofibril structures after 100 ns of simulation at 310 K, which served as the initial structures for pulling simulations: (a) wild-type, (b) F19G, (c) D23A, (d) K28A, and (e) I32G/L34G. All images include explicit stick representation of Asp23 and Lys28, unless mutated. Images rendered with PyMOL.[55]

TABLE 1: Backbone Rmsd Values after 100 ns of MD Simulation

system	backbone rmsd (Å), ±std dev
WT	2.65 ± 0.09
D23A	2.82 ± 0.07
I32G/L34G	3.93 ± 0.25
F19G	5.34 ± 0.17
K28A	5.93 ± 0.19

from membranes.[42] Application of an external force to cause displacement in the simulated system allows for the calculation of work, a path-dependent quantity. The use of this pulling force perturbs the equilibrium of the system, thus precluding the calculation of thermodynamic quantities directly from the SMD trajectory without large errors. Methods proposed by Jarzynski[43] and the weighted histogram analysis method (WHAM) of Kumar et al.[39] are commonly used to extract equilibrium data (free energies) from the nonequilibrium SMD trajectories for a more direct, quantitative means of comparing two systems. While Jarzynski's method requires running multiple SMD simulations, the WHAM procedure calculates ΔG from a number of simulations conducted on configurations generated from a single SMD simulation. We use the latter approach here.

By pulling on the COM of peptide A of the Aβ_{42} protofibril, force builds up until a breaking point is reached, at which time critical interactions are disrupted, allowing peptide A to dissociate from the core protofibril structure. In each of the protofibrils in this study, the point of maximum force corresponded to the instant just before the interpeptide backbone hydrogen bonds between Gly33 and Met35 of peptide A and the corresponding residues of peptide B were broken (Figure 4A), although the events leading up to the dissociation of each peptide differed, sometimes dramatically. It is for this reason that the force−time curves, generated by conducting COM pulling, by themselves are insufficient to conclusively determine the stability of each of the mutant protofibrils in this study (in

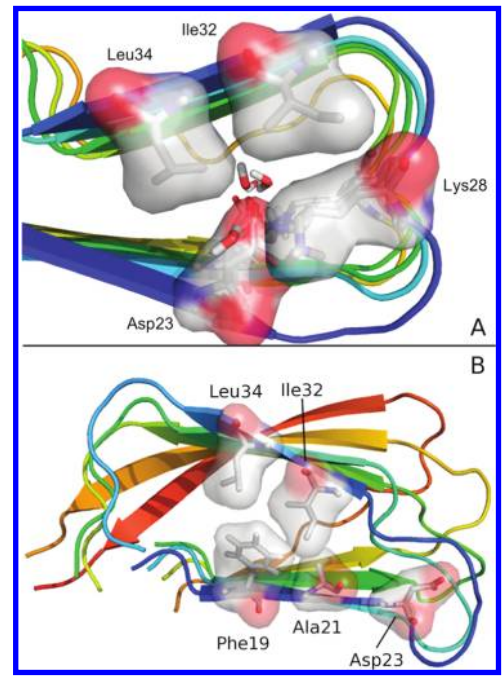

Figure 3. (A) Native packing of Ile32 and Leu34 against the Asp23−Lys28 salt bridge, taken from the WT protofibril configuration at the end of 100 ns of simulation. A narrow channel of water can be seen in the vicinity of the salt bridge. (B) Non-native packing in the K28A mutant protofibril, taken from the final configuration of the system (100 ns). Shown in detail are Phe19, Ala21, Asp23, Ile32, and Leu34 of peptide A. In the WT protofibril, Leu34 normally packs against the side chain of Asp23, and Ile32 with Lys28. Images rendered with PyMOL.[55]

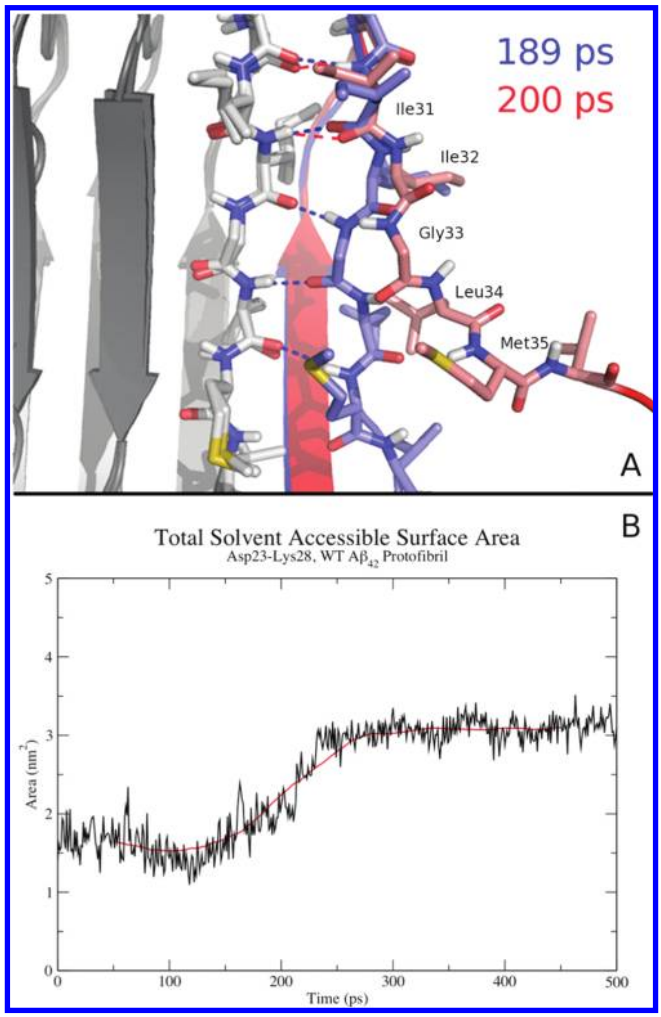

Figure 4. (A) Detail of the dissociation of peptide A from peptide B in the WT Aβ_{42} protofibril. Carbon atoms in peptide A are tinted blue (189 ps, the point of maximum force in Figure 3A) or red (200 ps, as the force is decreasing), while carbon atoms in peptide B are gray. Other elements are colored according to their typical representation (N, dark blue; O, dark red; H, white; S, yellow). Hydrogen bonds are indicated as dashed lines, colored according to the snapshot in which they occurred, demonstrating the interactions that are sequentially broken over the dissociation pathway. Image rendered with PyMOL.[55] (B) Total solvent-accessible surface area of the Asp23−Lys28 salt bridge of peptide A of the WT protofibril as the peptide is pulled away from the protofibril structure. The running average of the data (100-point windows) is shown in red to illustrate the overall trend in the data.

terms of ΔG), since the dissociation is a path-dependent process. Thus, the maximum force in each pulling simulation is not necessarily comparable to that of other simulations unless the dissociation pathway is very similar. Umbrella sampling[17−19] is employed to calculate the ΔG of binding of peptide A to each of these protofibrils considered here.

The mature Aβ_{42} fibril is stabilized by both intrapeptide (hydrophobic packing of β1 against β2) and interpeptide (backbone hydrogen bonding, salt bridges, and side-chain packing) interactions.[9] The use of COM pulling makes it possible to monitor the evolution of these types of interactions over time as peptide A is pulled away from the protofibril structure. Such a method serves a dual purpose here. It allows for qualitative assessment of the specific interactions that contribute to the stability of the protofibrils, and it generates a series of configurations that are used later for umbrella sampling.[17−19]

While the Asp23−Lys28 salt bridges in the Aβ_{42} fibril are primarily interpeptide interactions,[9] their stability may be influenced by a number of intrapeptide interactions, including the overall rigidity of the peptide structure induced by hydrophobic packing around the salt bridge and the interaction between the side chains of residues in β1 and β2. The terminal peptide (peptide A) may be especially influenced by this packing phenomenon, as an intrapeptide salt bridge is also capable of forming. That is, Asp23 of peptide A can be involved in two salt bridges simultaneously in the WT simulations described above—it can interact with both Lys28 of peptide B and Lys28 of peptide A. Both likely contribute to maintaining rigidity of the bend region, which, in turn, stabilizes the interaction of β1 and β2. We systematically explore these interactions in the following sections.

We begin the discussion of the COM pulling simulations with an analysis of the WT protofibril, which provides the rationale for in silico mutations that were made. We then describe the dissociation pathway of the mutant protofibrils, dividing them into two classes: those with intact Asp23−Lys28 salt bridges, and those without.

Wild-Type Aβ_{42} Protofibril. In the WT protofibril, after reaching the maximum force at 189 ps (blue structure in Figure 4A, blue line in Figure 5a), several intrapeptide packing interactions, Leu34 against Ala21 and Ile32 against the aliphatic portion of the Lys28 side chain, were both disrupted within only 11 ps (red structure in Figure 4A, red line in Figure 5a). These observations in the case of the WT protofibril highlight the importance of maintaining the packing of strand β2 (containing Ile32 and Leu34) against strand β1 (containing Asp23), especially in the vicinity of the Asp23−Lys28 salt bridge. The position of residues Ile32 and Leu34 define a narrow channel of water near the Asp23−Lys28 salt bridge (Figure 3A), allowing a finite level of hydration to persist near these charged residues. Mutation of Lys28 to alanine substantially perturbed this region (Figure 3A vs 3B, and discussed below). The presence of internal hydration in the Aβ_{42} fibril has been proposed previously.[23,44] Disruption of native packing in this region allowed additional water molecules to interact with the Asp23−Lys28 salt bridge, causing it to become increasingly exposed to bulk solvent (Figure 4B). Within approximately 60 ps after reaching the maximum force, the salt bridge was entirely exposed to bulk solvent (green line, Figure 5a). It appears that a delicate balance must be maintained in order to preserve a narrow channel of water that acts to stabilize the Asp23−Lys28 interaction, with water molecules serving as hydrogen bond bridges between these residues. If these interactions are disrupted, peptide A quickly moves away from peptide B. Thus, we generated a series of mutants (D23A, K28A, and I32G/L34G) to assess the contributions of the salt bridge and surrounding hydrophobic residues to the stability of the fibril as a whole. In addition, a mutant whose structure has been characterized experimentally (F19G) was analyzed.

The evolution of the protofibril in the SMD simulations was also examined using slower pulling rates (0.005 and 0.001 nm ps^{-1}) to verify that the faster pulling rate utilized (0.01 nm ps^{-1}) did not induce any artifacts. From Figure S1 (Supporting Information) it is clear that peptide A dissociated in the same manner under each of the applied pulling rates, giving effectively the same sequence of configurations, regardless of the pulling rate. The time required to achieve the maximum force, as well as the value of this maximum force, is dependent upon the pulling rate, as the structural changes are occurring at different rates. However, it is clear that a

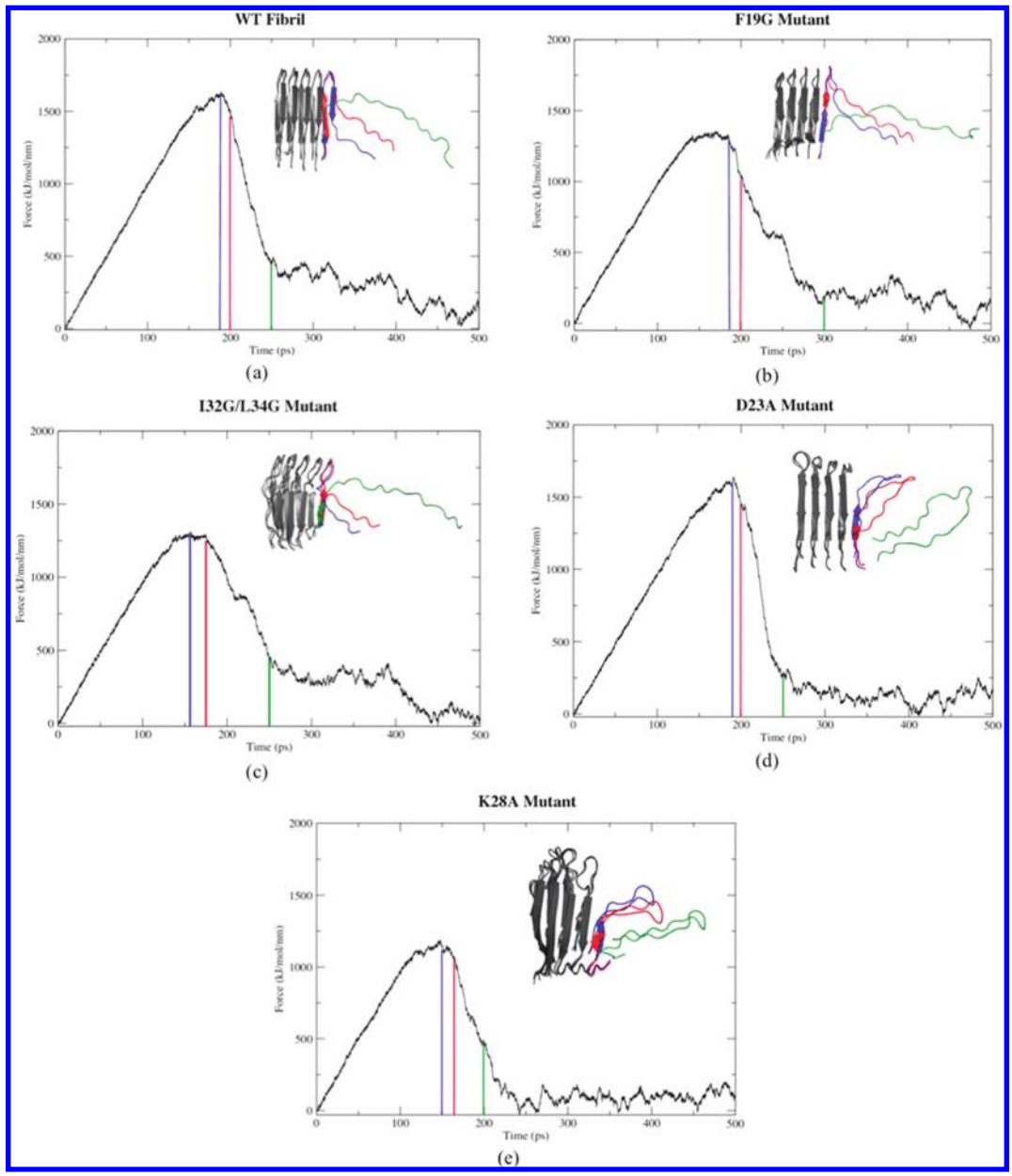

Figure 5. Dissociation pathways of Aβ_{42} protofibrils, with corresponding plots of force vs time: (a) WT, (b) F19G, (c) I32G/L34G, (d) D23A, and (e) K28A. In each panel, the blue line (and structure) corresponds to the point of maximum force, and the red and green lines and structures correspond to major structural transitions (WT, F19G, and I32G/L34G) or the dissociation of peptide A (D23A and K28A).

single main structural transition is produced in each case, corresponding to the pathway detailed above.

Mutant Protofibrils with Intact Salt Bridges (F19G and I32G/L34G). In the case of the mutant protofibrils that possessed intact salt bridges after 100 ns of MD simulation (F19G and I32G/L34G), applying force to peptide A resulted in dissociation pathways that largely followed that of the WT protofibril. Under the applied force, the C-terminal residues in the β2 region dissociated first, followed by the bend region and β1 for both F19G and I32G/L34G (Figure 5, b and c, respectively). For this reason, some general observations of the forces required to destabilize these protofibrils relative to the WT can be made, although a rigorous quantitative comparison of forces is not possible since the pathways are not identical.

The dissociation of peptide A in the F19G mutant required less force than in the case of the wild type. The F19G mutation does not alter the native packing in and around the salt bridge, although hydration is slightly decreased (5.1 water molecules per time frame) relative to the WT (6.8 water molecules per time frame) over the course of the 100 ns simulation conducted prior to pulling. The reduction in force thus derives from the non-native packing interactions that arise between strands β1 and β2 in F19G. The deletion of the Phe19 side chain (which normally packs against Gly38 in the WT structure) caused a bend in the backbone of β2 to generate a Gly19−Gly38 contact. This phenomenon strains the hydrogen bonds involving Val40 and Gly38, evidenced by the fact that less force is required to break them than in the case of the WT. The dissociation pathway of the F19G mutant resembled that of the WT protofibril, due largely to native packing of Ile32 and Leu34 against the Asp23−Lys28 salt bridge, with the narrow water channel described previously.

When Ile32 and Leu34 are simultaneously mutated to glycine, the bulky hydrophobic side chains that normally pack against β1 and the Asp23−Lys28 salt bridge are absent, such that when the hydrogen bonds involving Met35 break, there are fewer

stabilizing interactions in this region to preserve the interaction of peptides A and B. The Asp23−Lys28 salt bridge is also more solvent-accessible as a consequence. The greater extent of hydration around the salt bridge contributes to this destabilization, and peptide A is able to dissociate from peptide B with substantially less force than in the case of the WT protofibril.

Mutant Protofibrils without Intact Salt Bridges (D23A and K28A). To evaluate the contribution of the Asp23−Lys28 salt bridge to the binding of peptide A to the protofibril, both Asp23 and Lys28 were independently mutated to alanine. In the case of these mutants, peptide A dissociated from the protofibril along a dissociation pathway that was vastly different from that of the WT, F19G, and I32G/L34G structures, and thus the D23A and K28A mutants must be considered separately with respect to the nature of the forces required to cause this dissociation.

In the case of the D23A mutant, the predominantly polar bend region ($G_{25}SNKGA_{30}$) dissociates from the protofibril first (Figure 5d), likely due to the favorable exposure of Ser26, Asn27, and Lys28 to the aqueous solvent. Tight hydrophobic interactions between β-strands $\beta1$ and $\beta2$ (specifically Ile32−Ala23 and Leu34−Ala21) caused peptide A to remain compact as it dissociated from the rest of the protofibril structure. As interpeptide interactions in the $\beta1$ and $\beta2$ regions were simultaneously lost, the force, which was acting on both $\beta1$ and $\beta2$, decreased over a very short period of time (Figure 5d). Although the maximum force reached in both the WT and D23A pulling simulations is essentially identical (Figure 5, a and d, respectively), peptide A followed a very different dissociation pathway in each case. Specifically, the force applied to the COM of the WT peptide A produces a sequential dissociation of $\beta2$ and $\beta1$, while the same force applied to the D23A mutant acts to destabilize $\beta1$ and $\beta2$ simultaneously, following the dissociation of the bend region. Thus, conclusions cannot be made regarding the stability of these structures purely from an examination of this path-dependent quantity, but will be explored later using umbrella sampling.

In the case of the K28A mutant, Asp23 protrudes through the backbone of the bend region, contributing to the destabilization of the bend (Figure 2d), and leading to non-native packing (Figure 3B) prior to the application of any pulling force. The peak of the force curve (blue line, Figure 5e) corresponds to the disruption of interchain backbone hydrogen bonds involving Gly33 and Met35, as well as interpeptide Leu34 interactions, the side chains of which are also tightly packed against Phe19 and Ala21 in the core of the protofibril. Ile32 is also involved in this interaction in the K28A mutant, as the mutation destabilized the bend region and caused a shift in the alignment of the side-chain contacts (Figure 3B). Once this hydrophobic region is destabilized, the rest of peptide A quickly dissociated from the core of the protofibril. As was the case with the D23A mutant, peptide A dissociated in a compact conformation resembling a β-hairpin.

The structural rearrangements induced by the K28A and D23A mutations caused a shift in the contacts made between $\beta2$ residues and the central hydrophobic cluster (CHC, formed by packing between $\beta1$ and $\beta2$ in the region of residues $L_{17}VFFA_{21}$). When Lys28 is mutated, Ile32 and Leu34 shift their positions to interact with the $L_{17}VFFA_{21}$ sequence. Only a minor rearrangement is observed in the case of D23A, wherein Ile32 packs against the mutant Ala23 residue instead of the aliphatic portion of Lys28, which was exposed to solvent in the mutant structure. It appears from these observations that hydrophobic forces alone are insufficient to maintain the stability of the protofibril.

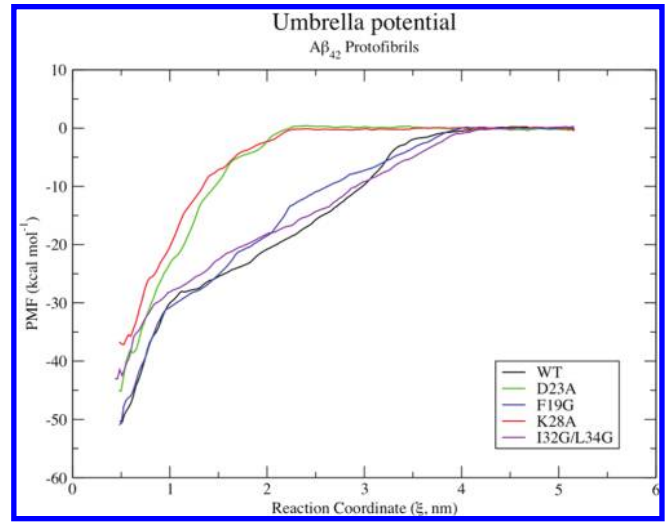

Figure 6. Potential of mean force (PMF) curve for each of the protofibrils in this study.

TABLE 2: Binding Free Energies for Wild-Type and Mutant Aβ Protofibrils

system	ΔG_{Bind} (kcal mol^{-1})[a]	$\Delta\Delta G_{Bind}$ (kcal mol^{-1})
WT	−50.5	−
F19G	−50.9	−0.4
D23A	−45.2	+5.3
I32G/L34G	−43.1	+7.1
K28A	−37.1	+13.4

[a] The error associated with energy minima is ±0.2 kcal mol^{-1} for each system.

Summary of Critical Interactions. The various mutations studied here illustrate the combination of hydrophobic and electrostatic forces that act to stabilize the Aβ_{42} protofibril. Mutations alter the native packing of the protofibril, highlighting the importance of regular side-chain packing both between peptides, and within peptide A, the $\beta1-\beta2$ interactions described above. From these COM pulling simulations, several important observations become clear: (i) the shape of the force curve and the magnitude of the maximum force (Figure 5) are dependent upon the dissociation pathway, but are also loosely correlated with the extent of structural perturbation induced by the mutation, as measured by backbone rmsd (Table 1), (ii) protection of the Asp23−Lys28 salt bridge from excess hydration (through packing interactions with Ile32 and Leu34, an interaction stabilized by Gly33 and Met35 interpeptide backbone hydrogen bonding, as well as Leu34−Ala21 intrapeptide packing) is important to the stability of the protofibril, and (iii) the absence of the Asp23−Lys28 salt bridge leads to the simultaneous dissociation of $\beta1$ and $\beta2$ of peptide A from the Aβ protofibril, in contrast to the WT pathway, wherein $\beta2$ and $\beta1$ dissociated sequentially under the influence of the applied force. It becomes clear that preserving the integrity of the Asp23−Lys28 salt bridge, and thus the rigidity of the bend region, largely governs the stability of the interaction between peptides in the Aβ_{42} protofibril.

Umbrella Sampling Simulations. Umbrella sampling simulations are used to determine the ΔG of a particular event along a reaction coordinate, ξ. In this case, the reaction coordinate corresponds to the z-axis, coincident with the Aβ protofibril axis. By using 31 sampling windows along this axis, one-dimensional potential of mean force (PMF) curves were obtained for each protofibril (Figure 6), leading to the ΔG of binding for peptide A in each of the protofibrils in this study (Table 2). Error

analysis was conducted using a bootstrap method described previously.[45] For the WT, F19G, D23A, and K28A PMF curves, the energy minimum occurred at a COM distance of 0.49−0.50 nm, in good agreement with WT peptide spacing determined by NMR.[9] For the I32G/L34G protofibril, the energy minimum is located at approximately 0.45 nm due to the fact that the double mutation allowed for closer interpeptide spacing because two bulky side chains were deleted.

Taking into account the magnitude of the standard error, mutation of Phe19 to glycine has no distinguishable effect on the free energy of binding between peptides A and B. In light of the fact that F19G mutant Aβ peptides form fibrils,[9] this result is not surprising. Though structurally distinct from the WT fibril, the F19G mutant can form stable interactions between peptides, leading to fibril formation. Mutating Asp23 or Lys28 to alanine, however, substantially destabilizes the protofibril, with the K28A mutation having a more profound effect (Table 2). It is clear from these results that disrupting the salt bridge, especially by increasing its exposure to solvent in the core of the Aβ_{42} protofibril, would likely destabilize the structure as a whole. This finding is corroborated by the PMF data for the I32G/L34G mutant. In this protofibril, the Asp23−Lys28 salt bridge is intact but exposed to a greater amount of solvent than in the WT protofibril. The $\Delta\Delta G$ of binding for the I32G/L34G mutant is +7.1 kcal mol^{-1}, indicating that the increased solvation of the salt bridge, through the loss of hydrophobic interactions that rigidify this region and define the solvent-accessible channel, leads to destabilization.

Discussion

Numerous simulations have been conducted on Aβ fragments,[26,27,46−48] monomeric full-length peptides,[49−52] protofilaments,[23,24] and fibrils,[20,21,25,38,44] but as of yet a detailed thermodynamic analysis of the factors influencing the stability of the Aβ_{42} fibril under physiologically relevant conditions is lacking. We sought to elucidate the effects of various mutations on the stability of the Aβ_{42} protofibril as a means to understand the contributions of various structural features (hydrophobic packing and the Asp23−Lys28 salt bridge) on the stability of the mature fibril. In order to properly account for electrostatic interactions, we conducted all simulations using explicit solvent, since many implicit solvent models fail to accurately represent these interactions.[26]

Previous simulations on the Aβ_{9-40} protofilament concluded that the stability of the mature Aβ fibril was due to inter- and intramolecular hydrophobic packing between the β-strands, as well as intermolecular Asp23−Lys28 salt bridges.[23] Contributing to the stability of the salt bridge is a region of internal hydration within the core of the fibril, a finding that extends to simulations conducted by Tarus et al.,[46] who found that, in the context of the Aβ_{21-30} fragment in solution, a single hydration shell favors the transient formation of the Asp23−Lys28 salt bridge over a competing Glu22−Lys28 salt bridge that may form in a more dehydrated environment. Increased solvation precludes the formation of stable salt bridges in the Aβ_{10-35} fragment.[26] Taken together with the results of replica-exchange MD simulations conducted by Melquiond et al.,[27] who reported that the strength of this salt bridge increases in dimeric structures relative to monomers, MD simulations indicate that the contribution of the Asp23−Lys28 salt bridge (both intra- and intermolecular) to the stability of Aβ aggregates increases with the size of the aggregate. Thus, it is reasonable to postulate that the Asp23−Lys28 salt bridge contributes significantly to the binding energy of an incoming Aβ peptide onto a growing Aβ fibril.

In our COM pulling simulations of the WT structure, the event precipitating the release of peptide A from the larger protofibril structure was the increased exposure of the Asp23−Lys28 salt bridge to solvent by destabilizing the β2 region extending from residues 32−35 ($I_{32}GLM_{35}$). It has been noted in several studies[23,44] that a narrow channel of water persists inside the Aβ fibril in the vicinity of the Asp23−Lys28 salt bridges, which we observe here, as well. Internal hydration near the Asp23−Lys28 salt bridge in the WT, F19G, and I32G/L34G structures persists over the course of the 100 ns trajectories conducted prior to pulling, with water molecules often bridging the amino and carboxylate functional groups of the respective side chains. When both Ile32 and Leu34 are mutated to glycine, additional water enters this channel, resulting in a weaker binding energy between peptides A and B. Thus, we propose that a delicate balance in the level of hydration of the salt bridge is key to its integrity. A small amount of water in the interior of the fibril stabilizes the Asp23−Lys28 interaction, but excess hydration of the salt bridge destabilizes it, allowing the Asp23 and Lys28 residues to interact with the bulk solvent. This event perturbs the bend region of peptide A, destabilizing the association between peptides A and B. This observation is also corroborated by the results of COM pulling simulations conducted on the D23A and K28A mutants. In these two simulations, salt bridges could not be formed, and the bend region of peptide A dissociated from that of peptide B very quickly, pulling the β1 and β2 regions away simultaneously. By using umbrella sampling, we have determined that independent mutations of Lys28 and Asp23 to alanine decrease the binding energy of the terminal peptide by 26.5% and 10.5%, respectively, relative to the WT protofibril. Increased hydration in this internal channel, as demonstrated in our I32G/L34G mutant, decreases the magnitude of the binding energy by 14.1%. All of these reduced binding affinities are a product of decreased native contacts and the resulting instability of the bend region.

Recent simulations of the Aβ protofilament structures (both Aβ_{40} and Aβ_{42}) concluded that the shape of the bend region influenced the packing behavior between the N-terminal and C-terminal β-strands.[25] Since the formation of this bend structure will dictate the nature of the hydrophobic contacts between the β-strands, its shape and the integrity of native packing may govern the stability of the fibril overall. Simulations of the A$\beta_{9-40/42}$ found that the formation of a stable bend between residues 23 and 28 ($D_{23}VGSNK_{28}$) could promote β-strand formation of the central hydrophobic cluster (CHC) located from residues 17−21 ($L_{17}VFFA_{21}$), which otherwise exists as a random coil in solution.[27] To analyze the importance of packing in the CHC and the bend region in protofibrils that are still salt bridge-competent, we generated two mutants, F19G and I32G/L34G. Despite deformations in the packing of β2 against the CHC (the Gly19−Gly38 contact and the resulting bend in the β2 region), native-like packing of Ile32 and Leu34 against the salt bridges is observed in the case of the F19G mutant, resulting in native-like internal hydration and a ΔG of binding between peptides A and B that is essentially the same as that of the WT protofibril. This result makes sense in light of the structural studies of Lührs et al., who determined that Aβ F19G mutant peptides could form fibrils, albeit morphologically distinct from those produced by WT Aβ.[9] The hydrophobic contacts involving Ile32 and Leu34 in the WT and F19G protofibrils are obviously absent in the I32G/L34G mutant, resulting in increased hydration of the Asp23−Lys28 salt bridges, a phenomenon that diminishes the magnitude of the binding energy of peptide A to peptide B.

If the Asp23−Lys28 salt bridge is perturbed, native side-chain contacts and packing in the CHC may not be preserved, and as a result, the protofibril structure is substantially less stable than in the case of the wild type. The packing interaction between the aliphatic portion of the Lys28 side chain with that of Ile32 aids in maintaining the necessary balance of hydration. Together with Leu34, the Ile32−Lys28 interaction defines a core region of stability in the Aβ_{42} fibril. Previous experimental work has determined that the weak hydrophobic interaction between the aliphatic portion of a lysine side chain and other hydrophobic amino acids such as tryptophan and isoleucine can contribute to the stability of β-hairpin peptides.[53,54] Our work is the first demonstration that this phenomenon is an important contribution to the stability of Aβ fibrils.

Conclusions

Using explicit solvent MD simulations, COM pulling, and umbrella sampling, we have demonstrated several key factors that are important to the stability of the Aβ_{42} fibril. In agreement with the results of Masman et al.,[24] we find that packing of the β2 region of the protofibril against β1, especially in the vicinity of the Asp23−Lys28 salt bridge, is important to the stability of the protofibril. Expanding upon those findings, we propose that residues Ile32 and Leu34 pack in the core of the fibril to help maintain the stability of the Asp23−Lys28 salt bridge by allowing a narrow channel of water to be present while simultaneously preventing overexposure of these charged residues to solvent. If Ile32 and Leu34 become destabilized, the salt bridge is disrupted and quickly solvated, as in the case of our I32G/L34G mutant. The absence of a stable salt bridge, modeled by our D23A and K28A mutants, leads to substantially reduced binding energy between the terminal peptide and its binding partner. Thus, we propose that compounds designed to either interfere with the hydrophobic packing interactions of residues Ile32 and Leu34 or directly disrupt the Asp23−Lys28 salt bridge may be viable therapeutic candidates to destabilize Aβ fibrils in the treatment of Alzheimer's disease.

Acknowledgment. The authors thank W. J. Allen for useful discussions regarding pulling simulations and the Terascale Computing Facility at Virginia Tech for computing time on the SystemX supercomputer. The material is based upon work supported by the Macromolecular Interfaces with Life Sciences (MILES) Integrative Graduate Education and Research Traineeship (IGERT) of the National Science Foundation under Agreement No. DGE-0333378, and by the Institute for Critical Technology and Applied Science (ICTAS) at Virginia Tech.

Supporting Information Available: Two additional figures are provided, the first showing the force vs time plots using different pulling rates and the second illustrating the evolution of side-chain contacts as the different protofibrils undergo β-strand twisting over time. This material is available free of charge via the Internet at http://pubs.acs.org.

References and Notes

(1) Saido, T. C.; Iwata, N. *Neurosci. Res.* **2006**, *54*, 235.
(2) Hardy, J. A.; Higgins, G. A. *Science* **1992**, *256*, 184.
(3) Haass, C.; Selkoe, D. J. *Nat. Rev. Mol. Cell Biol.* **2007**, *8*, 101.
(4) Selkoe, D. J. *Nature* **1999**, *399*, A23.
(5) Kayed, R.; Head, E.; Thompson, J. L.; McIntire, T. M.; Milton, S. C.; Cotman, C. W.; Glabe, C. G. *Science* **2003**, *300*, 486.
(6) Kayed, R.; Sokolov, Y.; Edmonds, B.; McIntire, T. M.; Milton, S. C.; Hall, J. E.; Glabe, C. G. *J. Biol. Chem.* **2004**, *279*, 46363.
(7) Lesné, S.; Koh, M. T.; Kotilinek, L.; Kayed, R.; Glabe, C. G.; Yang, A.; Gallagher, M.; Ashe, K. H. *Nature* **2006**, *440*, 352.
(8) Wasling, P.; Daborg, J.; Riebe, I.; Andersson, M.; Portelius, E.; Blennow, K.; Hanse, E.; Zetterberg, H. *J. Alzheimer's Dis.* **2009**, *16*, 1.
(9) Lührs, T.; Ritter, C.; Adrian, M.; Riek-Loher, D.; Bohrmann, B.; Döbeli, H.; Schubert, D.; Riek, R. *Proc. Natl. Acad. Sci. U.S.A.* **2005**, *102*, 17342.
(10) Deshpande, A.; Mina, E.; Glabe, C.; Busciglio, J. *J. Neurosci.* **2006**, *26*, 6011.
(11) Ono, K.; Hasegawa, K.; Yoshiike, Y.; Takashima, A.; Yamada, M.; Naiki, H. *J. Neurochem.* **2002**, *81*, 434.
(12) Ono, K.; Yoshiike, Y.; Takashima, A.; Hasegawa, K.; Naiki, H.; Yamada, M. *J. Neurochem.* **2003**, *87*.
(13) Bush, A. I. *Trends Neurosci.* **2003**, *26*, 207.
(14) Tycko, R. *Biochemistry* **2003**, *42*, 3151.
(15) Petkova, A. T.; Leapman, R. D.; Guo, Z.; Yau, W.-M.; Mattson, M. P.; Tycko, R. *Science* **2005**, *307*, 262.
(16) Paravastu, A. K.; Qahwash, I.; Leapman, R. D.; Meredith, S. C.; Tycko, R. *Proc. Natl. Acad. Sci. U.S.A.* **2009**, *106*, 7443.
(17) Patey, G. N.; Valleau, J. P. *Chem. Phys. Lett.* **1973**, *21*, 297.
(18) Torrie, G. M.; Valleau, J. P. *Chem. Phys. Lett.* **1974**, *28*, 578.
(19) Torrie, G. M.; Valleau, J. P. *J. Comput. Phys.* **1977**, *23*, 187.
(20) Takeda, T.; Klimov, D. K. *Biophys. J.* **2009**, *96*, 4428.
(21) Takeda, T.; Klimov, D. K. *Biophys. J.* **2009**, *96*, 442.
(22) Takeda, T.; Klimov, D. K. *Proteins: Struct. Funct. Bioinform.* **2009**, *77*, 1.
(23) Buchete, N.-V.; Tycko, R.; Hummer, G. *J. Mol. Biol.* **2006**, *353*, 804.
(24) Masman, M. F.; Eisel, U. L. M.; Csizmadia, I. G.; Penke, B.; Enriz, R. D.; Marrink, S. J.; Luiten, P. G. M. *J. Phys. Chem. B* **2009**, *113*, 11710.
(25) Miller, Y.; Ma, B.; Nussinov, R. *Biophys. J.* **2009**, *97*, 1168.
(26) Tarus, B.; Straub, J. E.; Thirumalai, D. *J. Am. Chem. Soc.* **2006**, *128*, 16159.
(27) Melquiond, A.; Dong, X.; Mousseau, N.; Derreumaux, P. *Curr. Alzheimer Res.* **2008**, *5*, 244.
(28) Oostenbrink, C.; Villa, A.; Mark, A. E.; van Gunsteren, W. F. *J. Comput. Chem.* **2004**, *25*, 1656.
(29) Darden, T.; York, D.; Pedersen, L. *J. Chem. Phys.* **1993**, *98*, 10089.
(30) Essmann, U.; Perera, L.; Berkowitz, M. L.; Darden, T.; Lee, H.; Pedersen, L. G. *J. Chem. Phys.* **1995**, *103*, 8577.
(31) Berendsen, H. J. C.; Postma, J. P. M.; van Gunsteren, W. F.; Hermans, J. Interaction models for water in relation to protein hydration. In *Intermolecular Forces*; Pullman, B., Ed.; Reidel: Dordrecht, The Netherlands, 1981; p 331.
(32) Berendsen, H. J. C.; Postma, J. P. M.; van Gunsteren, W. F.; DiNola, A.; Haak, J. R. *J. Chem. Phys.* **1984**, *81*, 3684.
(33) Nosé, S. *J. Chem. Phys.* **1984**, *81*, 511.
(34) Hoover, W. G. *Phys. Rev. A: At. Mol. Opt. Phys.* **1985**, *31*, 1695.
(35) Nosé, S.; Klein, M. L. *Mol. Phys.* **1983**, *50*, 1055.
(36) Parrinello, M.; Rahman, A. *J. Appl. Phys.* **1981**, *52*, 7182.
(37) Hess, B.; Kutzner, C.; van der Spoel, D.; Lindahl, E. *J. Chem. Theory Comput.* **2008**, *4*, 435.
(38) Takeda, T.; Klimov, D. K. *J. Phys. Chem. B* **2009**, *113*, 11848.
(39) Kumar, S.; Rosenberg, J. M.; Bouzida, D.; Swendsen, R. H.; Kollman, P. A. *J. Comput. Chem.* **1992**, *13*, 1011.
(40) Fawzi, N. L.; Kohlstedt, K. L.; Okabe, Y.; Head-Gordon, T. *Biophys. J.* **2008**, *94*, 2007.
(41) Kaminski, G. A.; Friesner, R. A.; Tirado-Rives, J.; Jorgensen, W. L. *J. Phys. Chem. B* **2001**, *105*, 6474.
(42) Izrailev, S.; Stepaniants, S.; Isralewitz, B.; Kosztin, D.; Lu, H.; Molnar, F.; Wriggers, W.; Schulten, K. *Steered Molecular Dynamics*; Springer-Verlag: Berlin, 1998; Vol. 4.
(43) Jarzynski, C. *Phys. Rev. Lett.* **1997**, *78*, 2690.
(44) Zheng, J.; Jang, H.; Ma, B.; Tsai, C.-J.; Nussinov, R. *Biophys. J.* **2007**, *93*, 3046.
(45) Hub, J. S.; de Groot, B. L. *Biophys. J.* **2006**, *91*, 842.
(46) Tarus, B.; Straub, J. E.; Thirumalai, D. *J. Mol. Biol.* **2008**, *379*, 815.
(47) Baumketner, A.; Bernstein, S. L.; Wyttenbach, T.; Lazo, N. D.; Teplow, D. B.; Bowers, M. T.; Shea, J.-E. *Protein Sci.* **2006**, *15*, 1239.
(48) Murray, M. M.; Krone, M. G.; Bernstein, S. L.; Baumketner, A.; Condron, M. M.; Lazo, N. D.; Teplow, D. B.; Wyttenbach, T.; Shea, J.-E.; Bowers, M. T. *J. Phys. Chem. B* **2009**, *113*, 6041.
(49) Flöck, D.; Colacino, S.; Colombo, G.; Di Nola, A. *Proteins: Struct. Funct. Bioinform.* **2006**, *62*, 183.
(50) Luttmann, E.; Fels, G. *Chem. Phys.* **2006**, *323*, 138.
(51) Sgourakis, N. G.; Yan, Y.; McCallum, S. A.; Wang, C.; Garcia, A. E. *J. Mol. Biol.* **2007**, *368*, 1448.
(52) Yang, M.; Teplow, D. B. *J. Mol. Biol.* **2008**, *384*, 450.
(53) Searle, M. S.; Griffiths-Jones, S. R.; Skinner-Smith, H. *J. Am. Chem. Soc.* **1999**, *121*, 11615.
(54) Tatko, C. D.; Waters, M. L. *J. Am. Chem. Soc.* **2004**, *126*, 2028.
(55) DeLano, W. L. *The PyMOL Molecular Graphics System*; DeLano Scientific LLC: Palo Alto, CA, 2009.

JP9110794